

Ultra High Fidelity Image Compression with ℓ_∞ -constrained Encoding and Deep Decoding

Xi Zhang and Xiaolin Wu, *Fellow, IEEE*

Abstract—In many professional fields, such as medicine, remote sensing and sciences, users often demand image compression methods to be mathematically lossless. But lossless image coding has a rather low compression ratio (around 2:1 for natural images). The only known technique to achieve significant compression while meeting the stringent fidelity requirements is the methodology of ℓ_∞ -constrained coding that was developed and standardized in nineties. We make a major progress in ℓ_∞ -constrained image coding after two decades, by developing a novel CNN-based soft ℓ_∞ -constrained decoding method. The new method repairs compression defects by using a restoration CNN called the ℓ_∞ -SDNet to map a conventionally decoded image to the latent image. A unique strength of the ℓ_∞ -SDNet is its ability to enforce a tight error bound on a per pixel basis. As such, no small distinctive structures of the original image can be dropped or distorted, even if they are statistical outliers that are otherwise sacrificed by mainstream CNN restoration methods.

More importantly, this research ushers in a new image compression system of ℓ_∞ -constrained encoding and deep soft decoding (ℓ_∞ -ED²). The ℓ_∞ -ED² approach beats the best of existing lossy image compression methods (e.g., BPG, WebP, etc.) not only in ℓ_∞ but also in ℓ_2 error metric and perceptual quality, for bit rates near the threshold of perceptually transparent reconstruction. Operationally, the new compression system is practical, with a low-complexity real-time encoder and a cascade decoder consisting of a fast initial decoder and an optional CNN soft decoder.

Index Terms—High fidelity image compression, ℓ_∞ -constrained encoding, deep soft decoding, light encoding and deep decoding

I. INTRODUCTION

In many professional applications of computer vision, such as medicine, remote sensing, sciences and precision engineering, high spatial and spectral resolutions of images are always of paramount importance. As the achievable resolutions of modern imaging technologies steadily increase, users are inundated by the resulting astronomical amount of image data. For example, a single pathology image generated by digital pathology slide scanner can easily reach the size of 1GB or larger. For the sake of operability and cost-effectiveness, images have to be compressed for storage and communication in practical systems.

Unlike in consumer applications, such as smartphones and social media, where users are mostly interested in image aesthetics, professionals of many technical fields are more concerned with the fidelity of decompressed images. Ideally, they want mathematically lossless image compression, that is,

the compression is an invertible coding scheme that can decode back to the original image, bit for bit identical. Although the mathematically lossless image coding is the ultimate gold standard, its compression performance is too limited. Despite years of research [1]–[5], typical lossless compression ratios for medical and remote sensing images are only around 2:1, which fall far short of the requirements of most imaging and vision systems.

In order to meet the stringent fidelity requirements while still achieving significant compression ratio, the ℓ_∞ -constrained (or colloquially called near-lossless) image coding methodology was developed [6]–[9] and standardized by ISO/JPEG [1], [10]. The distinction between the lossy and near-lossless compression methods is that the latter guarantees that at each pixel the absolute value of compression error is bounded by τ , τ being a user specified error tolerance. The tight per-sample error bound can only be realized by the minmax ℓ_∞ error criterion. The ubiquitous ℓ_2 error metric, which is adopted by consumer-grade lossy image compression methods, such as JPEG, JPEG 2000, WebP, etc., measures the average distortion over all pixels. The ℓ_2 compression is unable to preserve distinct image details that are statistical outliers but nevertheless vital to image semantics. Such cases are common in machine vision applications; for examples, one is searching in a big ocean for a small boat, or a small lesion in a large organ. When constrained by bit budget, an ℓ_2 -based lossy compression method tends to override such small structures by whatever dominant patterns in the background: ocean waves in the first example and liver textures in the second example. In order to avert such risks users (e.g., doctors, scientists and engineers) in many professions have to forego the ℓ_2 -based lossy compression widely used in consumer applications, and adopt the more conservative ℓ_∞ metric to keep compression error tolerance at a necessary minimum.

Since the standardization of the JPEG-LS nearlossless made in 1993, very little progress has been made in techniques for ℓ_∞ nearlossless image compression. Scheuch et al. and Zhou et al. realized that the per-pixel ℓ_∞ error bound offers much stronger and useful information than in the ℓ_2 -based compression, and used it to mitigate compression noises in a process called soft decoding [11]. Soft decoding of the ℓ_∞ -based nearlossless coded images is to solve the inverse problem of estimating the latent original image using the sparsity regularization and the prior knowledge of error bound τ . Although these methods are able to improve the precision of the compression reconstruction, their performances are limited by how well the assumed sparsity model fits the images in question. Any further progress in soft decoding has to come

X. Zhang is with the Department of Electronic Engineering, Shanghai Jiao Tong University, Shanghai, China (email: zhangxi_19930818@sjtu.edu.cn).

X. Wu is with the Department of Electrical & Computer Engineering, McMaster University, Hamilton, L8G 4K1, Ontario, Canada (email: xwu@ece.mcmaster.ca).

from adopting a more versatile and precise statistical model for the inverse problem, whatever complex and defying analytical tools it might turn out to be. The methodology of data-driven deep learning opens up such possibilities, as it can function as highly non-linear implicit statistical models.

Indeed, a large number of machine learning methods have been published recently for various image restoration tasks, including the reduction of compression noises [12]–[14]. However, these deep learning based methods for soft decoding are apparently motivated by consumer and Internet applications and heavily influenced by mainstream lossy image/video compression methods. They adopt ubiquitous ℓ_2 or ℓ_1 error metrics in the cost function of the restoration convolutional neural networks (CNN). This average fidelity design criterion tends to smooth out rare distinct image features. To counter the smoothing side effects, researchers widely adopt the technique of generative adversary neural network (GAN) for the task of compression artifacts removal. With an emphasis on pleasing visual appearances rather than high objective fidelity, GAN has a well-known tendency to fabricate "realistic" looking but false details in the reconstructed images. But any deletions and fabrications of image features are detrimental and should be absolutely forbidden in the professional fields of medicine, space, remote sensing, sciences, precision engineering and the alike.

One way to prevent the above identified side effects of minimizing the MSE loss and the GAN adversarial loss is the use of the ℓ_∞ loss function, when training the restoration CNN for compression artifact reduction or soft decoding. Unlike MSE and GAN losses, the ℓ_∞ loss imposes a tight error bound on each single pixel; therefore, it can preserve distinct and subtle structures of the original image even if they are statistical outliers. However, training the soft decoding CNN for minimum ℓ_∞ loss (called the ℓ_∞ -SDNet hereafter) may have convergence difficulties, if the image compressor is designed for ℓ_2 minimization as in current practice. For the feasibility of the ℓ_∞ -SDNet, we need to control the compression distortions at the source. The above reviewed ℓ_∞ -constrained image coding approach serves our purpose perfectly. The strict ℓ_∞ constraint of the encoder ensures each decoded pixel to have a given error bound τ , and consequently offers the ℓ_∞ -SDNet much needed strong priors to infer the inverse mapping of soft decoding.

The above reasoning leads to a novel ultra high-fidelity image compression system of ℓ_∞ -constrained encoding and deep soft decoding (ℓ_∞ -ED²), which is the main contribution of this work. In the ℓ_∞ -ED² system, an image is ℓ_∞ coded by a sequential prediction-quantization encoder; the decoder is a cascade of the conventional (hard) decoder and a deep soft decoder that is the ℓ_∞ -SDNet as outlined in the previous paragraph. As the strict non-differentiable ℓ_∞ loss does not permit backpropagation, we replace it with a differentiable quasi- ℓ_∞ loss term when optimizing the ℓ_∞ -SDNet; also we modify the activation function of the network and make it respond to the ℓ_∞ criterion, expediting the quasi- ℓ_∞ training process. In addition, we use the dilated convolution in the ℓ_∞ -SDNet to achieve larger receptive field with fewer layers. This makes the ℓ_∞ -SDNet shallower and more practical, while

reducing risk of overfitting.

The soft decoding network ℓ_∞ -SDNet outperforms the best of existing lossy image compression methods such as BPG, WebP, J2K, not only in ℓ_∞ but also in ℓ_2 error metric, for bit rates near the threshold of perceptually transparent reconstruction; in effect, it reduces the critical bandwidth for perceptually lossless image compression. The ℓ_∞ loss term contributes to the improved perceptual quality as ℓ_∞ penalizes the blurring of sharp edges more heavily than ℓ_2 .

Finally, we stress the practical significance of this research. The proposed ℓ_∞ -ED² image compression system not only raises the bar for achievable rate-distortion performance in ℓ_∞ , ℓ_2 error metrics and in perceptual quality, but more importantly it can realize the compression gain in real time encoding. This is simply because the ℓ_∞ -ED² system uses the traditional low complexity predictive encoder. Granted the CNN soft decoder ℓ_∞ -SDNet is more expensive than conventional predictive decoder, but it is an optional refinement after the quick hard decoding. The asymmetric complexity characteristic of the ℓ_∞ -ED² system gives it a distinct operational advantage over the recently researched end-to-end pure CNN compression approach [15]–[18], as the former has a lower encoding complexity than the latter by order of magnitude. Before a real-time CNN encoder of optimal rate-distortion performance can be economically implemented on end devices, such as cell phones, the ℓ_∞ -ED² system allows practitioners to reap the benefits of deep learning in practical image compression systems.

The remainder of this paper is structured as follows. Section II reviews the existing works for image compression artifacts removal. Section III outlines the proposed ℓ_∞ -ED² image compression system. Section IV presents technical details of the ℓ_∞ -constrained soft decoding network ℓ_∞ -SDNet. In Section V, details about the training of ℓ_∞ -SDNet are provided. In section VI, we report our experimental results in comparison with other competing methods on four datasets. Section VII concludes the paper.

II. RELATED WORKS

There is a rich body of literature on techniques for removing compression artifacts in images [12]–[14], [19]–[23]. The majority of the studies on the subject focus on postprocessing JPEG images to alleviate compression noises, apparently because JPEG is the most widely used lossy compression method. The published works can be classified into two categories: explicit model-based methods and data-driven learning-based methods.

In the first category, Reeve *et al.* [24] proposed to remove structured discontinuities of DCT code blocks by Gaussian filtering of the pixels around the DCT block boundaries. This work was improved by Zhai *et al.* [25] who performed postfiltering in shifted overlapped windows and fused the filtering results. A total minimum variation method constrained by the JPEG quantization intervals was used by Alter *et al.* [26] to reduce blocking artifacts and Gibbs phenomenon while preserving sharp edges. Bredies *et al.* [27] studied optimality conditions of the TV minimization approach in

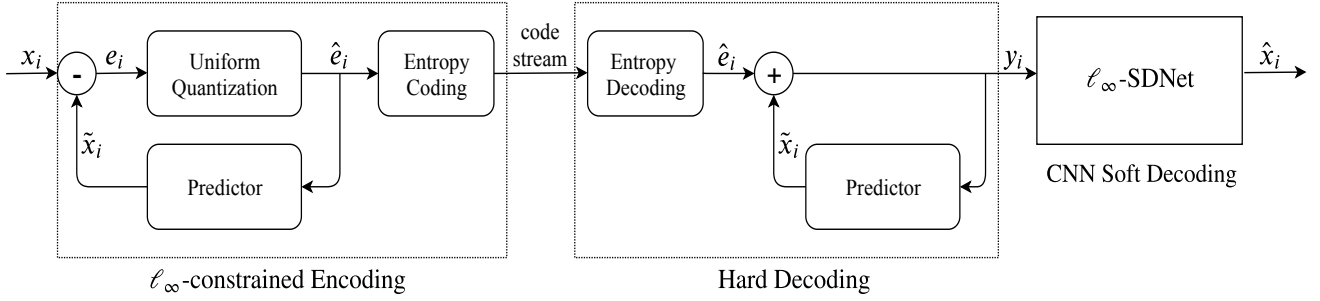


Fig. 1. Overall architecture of the ℓ_∞ -ED² image compression system. From left to right are the ℓ_∞ -constrained encoding module, conventional hard decoding module and deep soft decoding (ℓ_∞ -SDNet) module, respectively.

infinite dimension, and used a primal-dual algorithm to solve a discrete version. Li *et al.* [21] proposed to reduce compression artifacts by eliminating the artifacts that are part of the texture component, after decomposing images into structure and texture components. Zhang *et al.* [20] approached the problem by merging two predictions of DCT coefficients in each block: one prediction is derived from nonlocal blocks of DCT coefficients and the other from quantized values of DCT coefficients. Foi *et al.* [19] proposed to use attenuated DCT coefficients to estimate the local image signal under an adaptive shape support. Dar *et al.* [23] formulated the compression post-processing procedure as a regularized inverse-problem for estimating the original signal given its reconstructed form.

In the class of data-driven learning-based methods, an early approach is sparse coding. Chang *et al.* [22] proposed to use a sparse dictionary learnt from a training image set to remove the block artifacts. Liu *et al.* proposed a dual-dictionary method [28] carried out jointly in the DCT and pixel domains. Given the recent rapid development of deep convolutional neural networks (CNN), a number of CNN-based compression artifacts removal methods were published [12]–[14], [29]. Borrowing the CNN for super-resolution (SRCNN), Dong *et al.* [12] proposed an artifact reduction CNN (ARCNN). The ARCNN has a three-layer structure: a feature extraction layer, a feature enhancement layer, and a reconstruction layer. This CNN structure is designed in the principle of sparse coding. It was improved by Svoboda *et al.* [29] who combined residual learning and symmetric weight initialization. Zhang *et al.* [30] investigated the construction of feed-forward denoising convolutional neural networks (DnCNNs) in very deep architecture, learning algorithm, and regularization method into image denoising. Recently, Guo *et al.* [14] and Galteri *et al.* [13] proposed to reduce compression artifacts by Generative Adversarial Network (GAN), as GAN is able to generate sharper image details. It should be noted, however, that the GAN results may fabricate a lot of false hallucinated details, which is strictly forbidden in many scientific and medical applications.

To our best knowledge, the existing CNN-based image compression artifacts removal methods all focused on the JPEG post-processing, so we are the first to study the restoration of near-lossless compressed images.

III. THE ℓ_∞ -ED² IMAGE COMPRESSION SYSTEM

In this section we present the design principle and details of the ℓ_∞ -ED² image compression system. The system architecture is graphically depicted in Fig. 1.

First, we provide necessary background information on near-lossless image coding to facilitate the subsequent descriptions and understanding of our new work. In the literature, near-lossless image coding refers to the ℓ_∞ -constrained compression schemes that guarantee the compression error to be no larger than a user-specified bound for every pixel [9]. This is typically realized within the framework of classic predictive coding as illustrated in Fig. 1. We only need to describe the encoder algorithm, as the decoder simply reverses the encoder.

Denoting by X an image and x_i the value of pixel i , image X is compressed pixel by pixel sequentially, by first making a prediction of x_i :

$$\tilde{x}_i = F(C_i) \quad (1)$$

where C_i is a causal context that consists of previously coded pixels adjacent to x_i , and then entropy encoding and transmitting the prediction residual

$$e_i = x_i - \tilde{x}_i. \quad (2)$$

At the decoder side, x_i is recovered without any loss as $e_i + \tilde{x}_i$. However, to gain higher compression ratio, one can quantize e_i uniformly in step size τ to

$$\hat{e}_i = \begin{cases} (2\tau + 1) \lfloor (e_i + \tau) / (2\tau + 1) \rfloor & e_i \geq 0 \\ (2\tau + 1) \lfloor (e_i - \tau) / (2\tau + 1) \rfloor & e_i < 0 \end{cases} \quad (3)$$

In this way, the decoded pixel value becomes $y_i = \hat{e}_i + \tilde{x}_i$, with quantization error

$$\begin{aligned} d &= x_i - y_i \\ &= (e_i + \tilde{x}_i) - (\hat{e}_i + \tilde{x}_i) \\ &= e_i - \hat{e}_i \end{aligned} \quad (4)$$

But by Eq(3), the quantization error will be no greater than the bound τ for every pixel:

$$-\tau \leq x_i - y_i \leq \tau \quad (5)$$

The above inequalities not only impose an ℓ_∞ error bound, but more importantly they, for the purpose of this work, provide highly effective priors, on per pixel, to optimize the deep neural networks for deep decoding of the ℓ_∞ -compressed images.

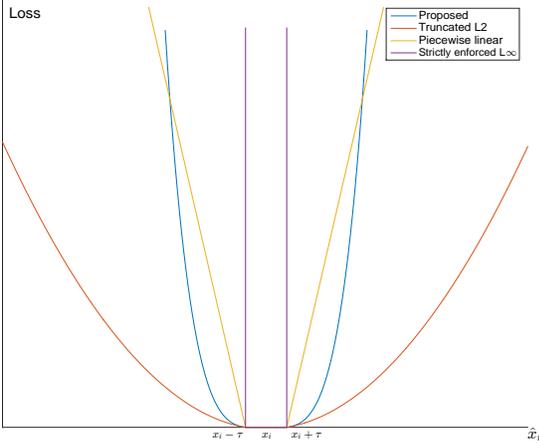


Fig. 2. True ℓ_∞ loss vs. its different approximations. **Purple curve**: true ℓ_∞ loss; **yellow curve**: piecewise linear approximation; **red curve**: truncated ℓ_2 loss; **blue curve**: the proposed quasi- ℓ_∞ loss.

IV. DESIGN OF ℓ_∞ -SDNET

A. Overview

Let A and A^{-1} be the encoder and decoder of an ℓ_∞ -constrained near-lossless compression algorithm A , such as CALIC [9], and let $Y = A^{-1}A(X)$ be the conventional decoded image of coding the original image X . The CNN restoration of the initially decoded image Y can be considered as a soft decoding process, aiming to refine Y and reconstruct an improved version \hat{X} by maximally removing compression artifacts in Y .

To solve the problem of compression artifacts removal, we train the ℓ_∞ -SDNet (denoted by G) that takes decompressed image Y as its input and generates the restored image $\hat{X} = G(Y)$. In order to satisfy the stringent fidelity requirements of medical and scientific applications, the final output image \hat{X} needs to be close to the original image X not only perceptually but also mathematically. To this end, we design our restoration network G with three new strategies. First, we incorporate a so-called quasi- ℓ_∞ error bound into the cost function $L_G(X, G(Y))$ in optimizing the network:

$$G = \arg \min_G \sum_{n=1}^N L_G(X_n, G(Y_n)), \quad (6)$$

for a given training dataset containing N training samples $\{(X_n, Y_n)\}_{1 \leq n \leq N}$. Second, we modify the activation function of the network and make it act on an ℓ_∞ criterion. This second strategy is to reinforce the ℓ_∞ loss term of the first strategy. The ℓ_∞ activation function has effects in both training and inference stages, while the quasi- ℓ_∞ loss function acts in the training only. Third, we build the network G by combining the encoder-decoder architecture and the dilated convolution, instead of the mainstream size-invariant fully convolutional network. This strategy is to achieve larger receptive field with fewer layers; the resulting shallower network has reduced risk of overfitting. These three new designs will be detailed in the following three subsections; also due to its ℓ_∞ properties we call the proposed network ℓ_∞ -SDNet.

B. Quasi- ℓ_∞ loss

The existing CNN methods for compression artifacts removal adopt the ubiquitous ℓ_2 loss function in optimizing the network:

$$L_2 = \frac{1}{WH} \sum_i (\hat{x}_i - x_i)^2 \quad (7)$$

where x_i and \hat{x}_i are the values of pixel i in X and \hat{X} , W and H are the width and height of X . Solely minimizing MSE seeks a good approximation in average sense, but it tends to smooth out distinctive image details which may be statistical outliers but have high semantic importance. To prevent the smoothing artifacts and preserve high frequency structures, we incorporate the ℓ_∞ fidelity criterion of near-lossless compression into the optimization of the ℓ_∞ -SDNet. For each pixel x_i in the restored image \hat{X} , the network objective function includes an ℓ_∞ loss term to heavily penalize the pixel values that are out of the range $[x_i - \tau, x_i + \tau]$, but not those within the range $[x_i - \tau, x_i + \tau]$. A simple way is to modify the ℓ_2 loss by making a flattened zero bottom portion of $[x_i - \tau, x_i + \tau]$, namely,

$$L_- = \frac{1}{WH} \sum_i \max((\hat{x}_i - x_i)^2 - \tau^2, 0) \quad (8)$$

However, this truncated ℓ_2 loss is not steep enough outside the interval $[x_i - \tau, x_i + \tau]$ (see red curve in Fig. IV-B); the penalties for pixel values beyond the user specified tolerance level are still too small.

If strictly enforced the ℓ_∞ loss should be infinity outside the interval $[x_i - \tau, x_i + \tau]$ (purple curve in Fig. IV-B). However, when optimizing the network we cannot back-propagate the errors of the strict ℓ_∞ loss function since it is not differentiable outside the interval $[x_i - \tau, x_i + \tau]$. The difficulty can be circumvented by modifying the ℓ_∞ loss function as a pair of steep slope lines arising from the ends of interval $[x_i - \tau, x_i + \tau]$ (yellow curve in Fig. IV-B). As the modified ℓ_∞ loss is a piecewise linear function, back propagation becomes possible. Still some cautions are needed about the slope steepness; too steep a slope of the piecewise linear approximation of ℓ_∞ may penalize the values slightly exceeding the range $[x_i - \tau, x_i + \tau]$ too heavily, causing the training of the ℓ_∞ -SDNet to be unstable and difficult to converge.

To approximate the ℓ_∞ norm closely but without convergence difficulties, we propose a quasi- ℓ_∞ loss term:

$$L_\infty = \frac{1}{WH} \sum_i \max((\hat{x}_i - x_i)^4 - \tau^4, 0) \quad (9)$$

As illustrated in Fig. 2, the quasi- ℓ_∞ loss (blue curve) remains zero within the range $[x_i - \tau, x_i + \tau]$, but it rises once the pixel value drifts away from the range, and the rate of penalty increase is much higher than the truncated ℓ_2 loss (red curve). When only slightly beyond the range $[x_i - \tau, x_i + \tau]$, the quasi- ℓ_∞ penalty is milder than the piecewise linear version (yellow curve), and it jumps far more rapidly than the latter if the pixel value deviates any further. Optimizing the ℓ_∞ -SDNet under the quasi- ℓ_∞ error metric forces the inference results to have a tight error bound on each pixel, while the training has a good convergence behaviour.

We combine the ℓ_2 loss and the quasi- ℓ_∞ loss to optimize the proposed ℓ_∞ -SDNet. The joint loss function is defined as:

$$L_G = L_2 + \lambda L_\infty \quad (10)$$

where λ is the hyper-parameter, which is set to 0.2 in our experiments.

C. Truncated activation

As the definition of the quasi- ℓ_∞ loss requires the knowledge of the ground truth value x_i , it can only be applied in the training stage not in the inference stage. If the ℓ_∞ -SDNet operates on compressed images whose statistics does not match the distribution of the training images, it may not guarantee the ℓ_∞ tight error bound on every pixel. In order to strengthen the control of restoration errors of the ℓ_∞ -SDNet and improve its generalization ability, we design a novel activation function for the last layer of neurons in our network.

Given the error bound τ of near-lossless compression algorithm and the decompressed image Y , according to Eq(5), the reconstructed image \hat{X} should satisfy the following constraint:

$$y_i - \tau \leq \hat{x}_i \leq y_i + \tau \quad (11)$$

where index i traverses all pixels in \hat{X} and Y . So, in order to ensure that \hat{X} can satisfy such constraints in Eq. 11, we need to clip the output \tilde{X} of the ℓ_∞ -SDNet to generate \hat{X} , by

$$\hat{x}_i = T(\tilde{x}_i) = \begin{cases} y_i - \tau, & \tilde{x}_i < y_i - \tau \\ \tilde{x}_i, & y_i - \tau \leq \tilde{x}_i \leq y_i + \tau \\ y_i + \tau, & \tilde{x}_i > y_i + \tau \end{cases} \quad (12)$$

where \tilde{x}_i is the value of pixel i in \tilde{X} . The proposed truncation function can be implemented as a piecewise linear activation function embedded in the neural network. In the last layer of the ℓ_∞ -SDNet, the activation function for each pixel is piecewise linear, similar to ReLU. The derivative of the truncated function is:

$$T'(\tilde{x}_i) = \begin{cases} 0, & \tilde{x}_i < y_i - \tau \\ 1, & y_i - \tau \leq \tilde{x}_i \leq y_i + \tau \\ 0, & \tilde{x}_i > y_i + \tau \end{cases} \quad (13)$$

Note that y_i is available from the decompressed image Y , so the truncation activation can be applied not only in the training phase, but also in the inference phase. This truncated activation guarantees that the output of the ℓ_∞ -SDNet \hat{x}_i falls into the interval $[y_i - \tau, y_i + \tau]$, and according to Eq. 5, y_i is in $[x_i - \tau, x_i + \tau]$, so the reconstructed \hat{x}_i must satisfy:

$$-2\tau \leq \hat{x}_i - x_i \leq 2\tau \quad (14)$$

The significance of the above analysis is that the restored image enjoys an error bound 2τ on a per pixel basis even in the worst case.

D. Network Architecture

Recent works show that deeper and wider neural network architectures can achieve superior results in image restoration tasks [30]–[35], as they have sufficient capacity to learn a highly complex mapping. Although removing compression noises is an image restoration problem, the compression noises are a well understood prior, and moreover in our case the distortion of the ℓ_∞ -constrained compression is tightly bounded. As a result, the mapping from decoded images to lossless counterparts should be simpler than in general denoising and other restoration tasks. For this reason the existing deep networks such as EDSR are not ideally suited to our task, because too many convolution layers not only incur high computational costs but are also prone to over-fitting risk.

In the design of our ℓ_∞ -SDNet, we try to make the network as simple as possible. It contains 8 residual blocks [36], not like 16 or 32 residual blocks used in existing image restoration CNNs. However, reducing residual blocks narrows the receptive field, i.e., incapable to capture higher order statistical dependencies among pixels. This weakness is countered by two measures. Firstly, we adopt an encoder-decoder architecture for the ℓ_∞ -SDNet with down-sampling and up-sampling operators, instead of a size-invariant fully convolutional architecture as in the mainstream design of image restoration networks. Given the network depth, the former has a larger receptive field than the latter due to the down-sampling operation.

Secondly, in each residual block, we replace the traditional convolutional layers with the dilated convolution layers [37]–[39]. By combining the encoder-decoder architecture and the dilated convolution, the proposed ℓ_∞ -SDNet can achieve the same or larger receptive field as other networks, but with fewer layers. The overall architecture of the proposed ℓ_∞ -SDNet is illustrated in Fig. 3 and the details of the residual block architecture are illustrated in Fig. 4. The dilation factor is set to 2 in our design.

V. TRAINING OF MULTI-RATE ℓ_∞ -SDNET

In this section, we present the details of training the proposed ℓ_∞ -SDNet for deep decoding of ℓ_∞ -compressed images, including how to train the ℓ_∞ -SDNet for multiple compression bit rates so that it becomes universal and applicable on a wide range of bit rates (compression ratios).

A. Training data and settings

In the existing works on CNN-based compression artifacts removal [12]–[14], data used for training are from the popular datasets like BSD100, ImageNet or MSCOCO. But images in these datasets are already compressed and have relatively low resolutions, hence they are not suitable as the ground truth for our purpose of ultra high fidelity image decompression for professional applications. Instead, we choose the high-quality uncompressed image dataset DIV2K for training. The DIV2K dataset consists of 2K resolution images and is commonly used to synthesize paired training images for the construction of image restoration CNNs. To generate compressed and original image pairs to train the above proposed ℓ_∞ -SDNet, we use

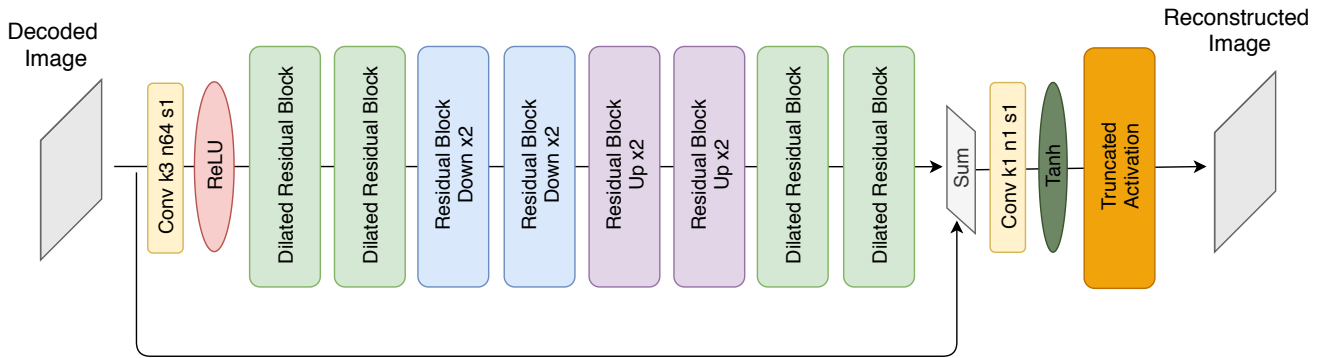


Fig. 3. Overall architecture of the proposed ℓ_∞ -SDNet with kernel size (k), number of feature maps (n) and stride (s).

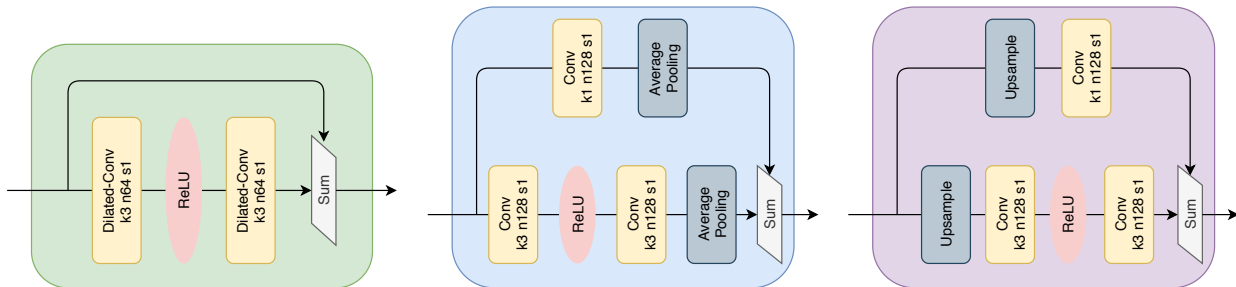


Fig. 4. Detailed architectures of the dilated residual block (left), downsampled residual block (middle) and upsampled residual block (right).

the ℓ_∞ -constrained (near-lossless) CALIC algorithm [9] to compress the DIV2K images with a given error bound τ for every pixel ($\tau = 1, 2, 3, 4, 5, 6, 7, 8$ used in our experiments).

The DIV2K high resolution images are of consumer RGB type. We carry out our experiments on the Y (luminance) channel of the DIV2K images because the Y channel has the most information (highest entropy) and hence most difficult to compress. Here we deliberately challenge ourselves by using high resolution consumer monochrome images to train the ℓ_∞ -SDNet, but carrying out inferences beyond the DIV2K dataset, including some satellite images.

The training images are decomposed into 128×128 sub-images with stride 32, after compressed by the near-lossless CALIC algorithm. We train the proposed ℓ_∞ -SDNet with Adam optimizer [40] by setting momentum term $\beta_1 = 0.9$ and $\beta_2 = 0.999$. The neural network is trained with 100 epochs at the learning rate of 10^{-4} and other 50 epochs with learning rate of 10^{-5} . We implement the proposed model in TensorFlow [41] and train it with 4 NVIDIA TITAN Xp GPUs.

B. Multi-rate Training

In previous CNN-based methods for compression artifacts removal, the training is carried out only with respect to a single compression bit rate. For instance, the training images are all of the same quality factor (QF) of the JPEG compression standard. Needless to say, the CNN learned for a given QF may not work well for images compressed in different QF's. Alternatively, many QF-specific CNNs can be trained for different QF's, but this approach is inefficient in practice. In this work, we train a unified ℓ_∞ -SDNet for restoring images compressed in a range of bit rates. Each image in the training

set is compressed for different, from low to high compression ratios, or for increasing ℓ_∞ bounds $\tau = 1, \dots, 8$. Thus, each patch in the original image has multiple compressed versions of different qualities, forming multiple sample pairs; all of them participate in the training of the multi-rate ℓ_∞ -SDNet. It turns out, as shown in the ablation study section, that the resulting multi-rate ℓ_∞ -SDNet is more robust than the single-rate counterpart. The multi-rate ℓ_∞ -SDNet even outperforms the single-rate ℓ_∞ -SDNet on testing images that are compressed at the said single rate.

VI. PERFORMANCE EVALUATION

We have implemented the proposed ℓ_∞ -SDNet for the task of removing compression artifacts, and conducted extensive experiments of near-lossless image decompression with it. Recall that our objective is to achieve the best possible compression rate-distortion performance at the threshold of perceptually lossless quality by coupling the CNN decoding and the ℓ_∞ -constrained predictive encoding of images. To establish our claim, we compare our results with those of three popular lossy image compression methods: JPEG 2000 [42], WebP [43] and BPG [44] in both ℓ_∞ and ℓ_2 distortion metrics when they operate at perceptually lossless quality level.

JPEG 2000 is an image compression standard created by the Joint Photographic Experts Group committee in 2000 with the intention of superseding the original JPEG standard. WebP is an image format developed by Google, announced in 2010 as a new open standard for image compression. BPG is the state-of-the-art image lossy compression method of the best performance so far. It is based on the intra-frame encoding of the High Efficiency Video Coding (HEVC) video compression



Fig. 5. Sample images of the Aerial dataset.

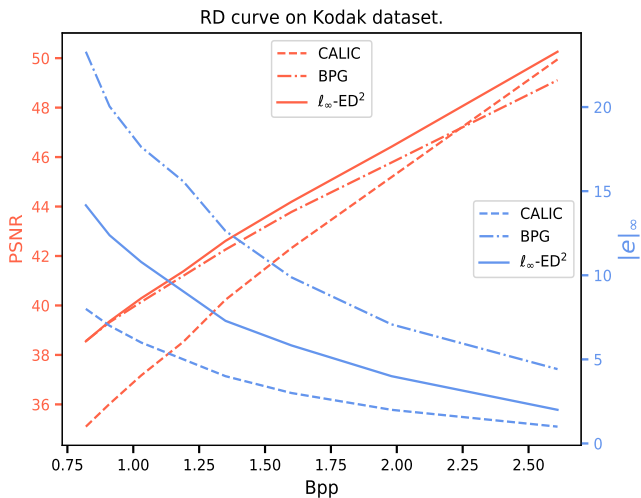


Fig. 6. PSNR and $\|e\|_\infty$ of the competing methods on the the Kodak dataset.

standard. Also, we include in our comparison group the deep learning method DnCNN that can be applied for compression artifact removal [30]. The DnCNN is trained with the same DIV2K and the near-lossless CALIC-compressed image pairs, as in the training of the proposed ℓ_∞ -SDNet.

Although the CNN decompression methods are trained by the DIV2K dataset, they and the other non-CNN methods are tested on four different test image sets LIVE1 [45], Kodak [46] and Urban [47] and a set of aerial and satellite image. The first three test image sets are widely used in literature for evaluating image restoration methods. The last test set has 22 high-resolution aerial and satellite images, which are typical of those in remote sensing and other professional applications. Some sample images from the set are shown in Fig. 5.

A. Quantitative evaluation

To facilitate fair rate-distortion performance evaluations, for each test image, the rates of JPEG2000, WebP and BPG are adjusted to match that of the near-lossless CALIC. Given the rate, both ℓ_∞ and ℓ_2 (PSNR) distortion metrics are used to measure the image quality of different methods. The ℓ_∞ error is defined as follow:

$$\|e\|_\infty = \max(|\hat{x}_i - x_i|) \tag{15}$$

Rate-distortion performance results of the competing methods are tabulated in Tables II, III, IV, V, for the four test sets respectively. Note the reported value of $\|e\|_\infty$ is the average for the corresponding test set. As shown in the four

TABLE I
MODEL SIZE AND INFERENCE TIME FOR A 1024×1024 IMAGE IN GPU.

	DnCNN [30]	ℓ_∞ -SDNet
Model size (MB)	2.24	1.08
Inference time (s)	0.22	0.08

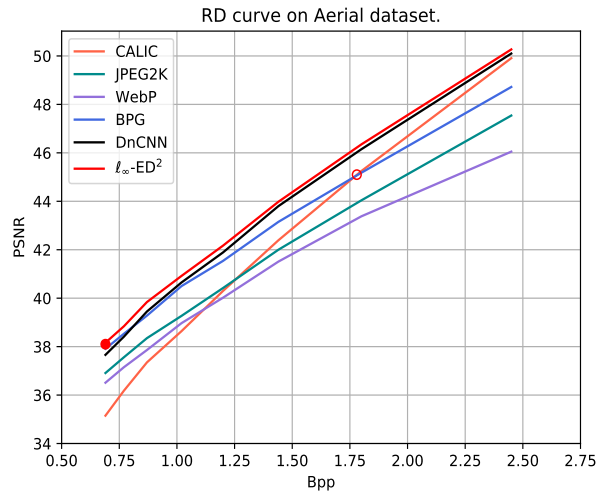


Fig. 7. Rate-distortion curves of the competing methods on the Aerial dataset.

tables, the proposed ℓ_∞ -ED² system outperforms all lossy compression methods JPEG2000, WebP and BPG consistently, not only in PSNR but also in $\|e\|_\infty$, for bit rate larger than 0.8 bpp (roughly the threshold of perceptually transparent reconstruction). At the same time, the proposed ℓ_∞ -SDNet also beats the CNN-based denoising model DnCNN in both PSNR and $\|e\|_\infty$. It is noteworthy that the former has the smaller model size and faster inference speed than the latter. Table I shows that the ℓ_∞ -SDNet is only half the size of DnCNN and its inference speed is three times faster.

Fig. 6 plots the PSNR (left Y axis) and $\|e\|_\infty$ (right Y axis) of different methods vs. bit rate for the Kodak dataset (the patterns are similar for other datasets). The near-lossless CALIC is the best in the ℓ_∞ norm, but the worst in the ℓ_2 norm (PSNR). The proposed deep decoding technique greatly improves the PSNR of CALIC while still maintaining a relatively tight ℓ_∞ error bound on each pixel. More importantly, the ℓ_∞ -ED² system method achieves higher PSNR than the BPG method for bit rates near and above the threshold of perceptually transparent reconstruction (bpp > 0.76, PSNR < 38); at the same time its $\|e\|_\infty$ is only half of the latter. This is quite remarkable considering BPG is optimized for ℓ_2 and it is considered the best PSNR performer up to now.

Fig. 7 graphically represent the rate-distortion behaviours of different methods for the Aerial dataset (the patterns are similar for other datasets). In terms of compression methodology, JPEG 2000, WebP and BPG are transform based coding, while CALIC is predictive coding. Before this work the consensus is that predictive coding outperforms transform coding only for very high bit rates (low compression ratio), hence it is suited

TABLE II
PERFORMANCE RESULTS (PSNR/ $\|e\|_{\infty}$) OF THE COMPETING METHODS ON THE LIVE1 DATASET.

Bit rate (bpp)	CALIC	JPEG2000	WebP	BPG	DnCNN	ℓ_{∞} -ED ²
2.78	49.93 / 1.00	47.76 / 5.51	45.73 / 6.31	48.99 / 4.38	50.14 / 2.00	50.23 / 2.00
2.15	45.19 / 2.00	44.36 / 8.72	43.39 / 9.38	45.42 / 7.24	46.12 / 4.00	46.28 / 4.00
1.76	42.31 / 3.00	42.35 / 11.76	41.41 / 12.34	43.26 / 10.34	43.68 / 6.00	43.92 / 5.82
1.50	40.20 / 4.00	40.64 / 14.51	40.00 / 14.89	41.72 / 12.86	42.02 / 7.82	42.25 / 7.20
1.31	38.49 / 5.00	39.41 / 16.72	38.83 / 17.80	40.49 / 15.76	40.63 / 9.79	40.91 / 9.03
1.15	37.13 / 6.00	38.32 / 20.66	38.11 / 19.10	39.47 / 19.24	39.49 / 11.88	39.79 / 10.86
1.03	35.98 / 7.00	37.39 / 24.93	36.92 / 24.41	38.65 / 20.90	38.45 / 13.82	38.81 / 12.20
0.94	35.05 / 8.00	36.62 / 26.34	36.55 / 24.28	37.91 / 23.93	37.66 / 15.76	38.05 / 14.01

TABLE III
PERFORMANCE RESULTS (PSNR/ $\|e\|_{\infty}$) OF THE COMPETING METHODS ON THE KODAK DATASET.

Bit rate (bpp)	CALIC	JPEG2000	WebP	BPG	DnCNN	ℓ_{∞} -ED ²
2.61	49.95 / 1.00	47.96 / 5.21	45.86 / 6.33	49.11 / 4.42	50.15 / 2.00	50.26 / 2.00
1.98	45.19 / 2.00	44.76 / 8.42	43.74 / 8.92	45.78 / 7.08	46.25 / 4.00	46.42 / 4.00
1.60	42.32 / 3.00	42.78 / 11.58	41.91 / 11.80	43.78 / 9.88	43.97 / 6.00	44.19 / 5.83
1.35	40.23 / 4.00	41.20 / 14.12	40.55 / 14.42	42.26 / 12.63	42.35 / 8.00	42.61 / 7.29
1.19	38.53 / 5.00	40.07 / 15.80	39.53 / 16.33	41.20 / 15.58	41.11 / 9.92	41.38 / 9.04
1.03	37.17 / 6.00	38.98 / 19.46	38.53 / 19.54	40.14 / 17.63	39.96 / 11.84	40.29 / 10.79
0.91	36.02 / 7.00	38.11 / 24.38	37.67 / 22.50	39.32 / 20.04	38.98 / 13.79	39.36 / 12.38
0.82	35.10 / 8.00	37.31 / 27.10	36.99 / 24.41	38.56 / 23.29	38.12 / 15.80	38.55 / 14.16

TABLE IV
PERFORMANCE RESULTS (PSNR/ $\|e\|_{\infty}$) OF THE COMPETING METHODS ON THE URBAN100 DATASET.

Bit rate (bpp)	CALIC	JPEG2000	WebP	BPG	DnCNN	ℓ_{∞} -ED ²
2.66	49.97 / 1.00	47.74 / 5.76	45.94 / 6.92	49.34 / 4.20	50.29 / 2.00	50.42 / 2.00
2.06	45.30 / 2.00	44.18 / 9.51	43.23 / 10.35	45.33 / 7.10	46.32 / 4.00	46.47 / 4.00
1.71	42.38 / 3.00	42.00 / 13.43	41.28 / 13.38	43.22 / 9.71	43.93 / 6.00	44.12 / 5.93
1.45	40.24 / 4.00	40.15 / 16.21	39.72 / 16.76	41.82 / 13.16	42.19 / 7.95	42.44 / 7.57
1.28	38.54 / 5.00	38.84 / 20.39	38.44 / 20.24	40.73 / 16.11	40.86 / 9.80	41.14 / 9.20
1.13	37.17 / 6.00	37.67 / 24.50	37.35 / 23.84	39.75 / 19.58	39.74 / 11.75	40.02 / 11.02
1.02	36.01 / 7.00	36.69 / 28.54	36.46 / 27.14	38.82 / 22.80	38.61 / 13.88	39.04 / 12.70
0.94	34.96 / 8.00	35.92 / 31.64	35.84 / 29.63	38.12 / 25.91	37.86 / 15.82	38.32 / 14.38

TABLE V
PERFORMANCE RESULTS (PSNR/ $\|e\|_{\infty}$) OF THE COMPETING METHODS ON THE AERIAL DATASET.

Bit rate (bpp)	CALIC	JPEG2000	WebP	BPG	DnCNN	ℓ_{∞} -ED ²
2.45	49.91 / 1.00	47.54 / 5.41	46.05 / 5.90	48.72 / 4.27	50.10 / 2.00	50.27 / 2.00
1.80	45.25 / 2.00	44.04 / 8.02	43.38 / 8.95	45.18 / 7.10	46.15 / 4.00	46.35 / 3.77
1.44	42.39 / 3.00	42.00 / 11.50	41.51 / 11.45	43.15 / 9.23	43.80 / 5.92	43.98 / 5.36
1.20	40.30 / 4.00	40.42 / 13.77	40.02 / 14.68	41.54 / 12.41	41.89 / 7.80	42.17 / 7.13
1.02	38.64 / 5.00	39.27 / 16.63	38.97 / 16.50	40.50 / 14.63	40.65 / 9.76	40.92 / 8.82
0.87	37.35 / 6.00	38.35 / 19.95	37.86 / 19.95	39.28 / 17.45	39.51 / 11.78	39.84 / 10.59
0.77	36.18 / 7.00	37.56 / 23.27	37.15 / 22.13	38.53 / 21.02	38.41 / 13.60	38.84 / 12.23
0.69	35.15 / 8.00	36.91 / 26.81	36.51 / 24.72	37.91 / 22.68	37.66 / 15.62	38.16 / 13.95

for lossless but not for lossy compression. The above long held view has been now changed by the ℓ_{∞} -ED² system. As shown in Fig. 7, the CNN soft decoding of predictive coded images outperforms all transform coding methods, including the state-of-the-art BPG method. Without the CNN soft decoding, the rate-distortion curves of the transform coding method BPG and the predictive coding method CALIC cross each other at 1.76 bpp. With the CNN soft decoding, the cross over

point moves to a much lower bit rate of 0.73 bpp. These findings suggest that the best practical strategy for perceptually transparent lossy image compression is the ℓ_{∞} -constrained predictive encoding followed by the CNN soft decoding. This strategy allows us to use a low complexity encoder for real time image acquisition and a fast preview decoder, while still having the option to achieve the original quality with a tight per pixel error bound.

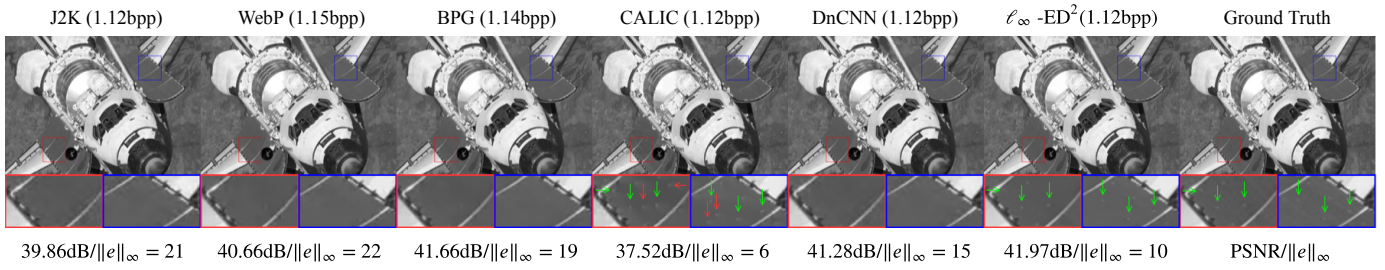


Fig. 8. Visual comparisons of different methods. The second row presents close-up views. Notice how the nuts (green arrows) on the hatch are erased by J2K, WebP, BPG, DnCNN but preserved by ℓ_∞ -ED², and how the errors (red arrows) of CALIC are corrected by ℓ_∞ -ED².

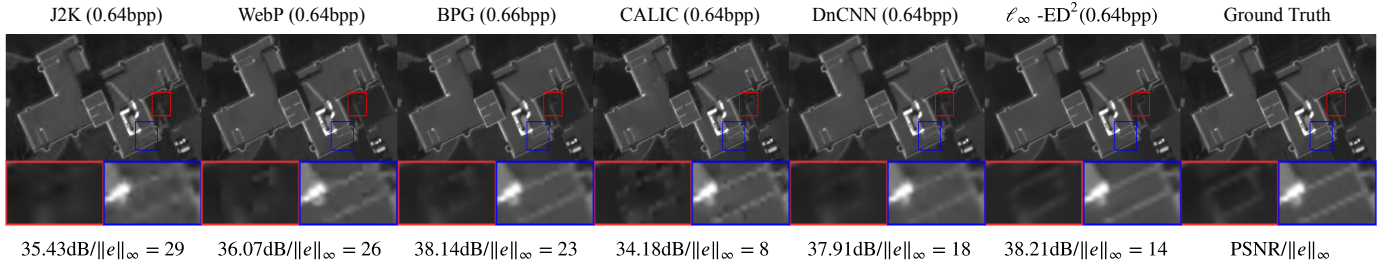


Fig. 9. Visual comparisons of different methods. Note the erasures and distortions of line structures by J2K, WebP, BPG, CALIC and DnCNN in comparison with ℓ_∞ -ED² in close-up views, and also the correction of CALIC distortions by ℓ_∞ -ED².

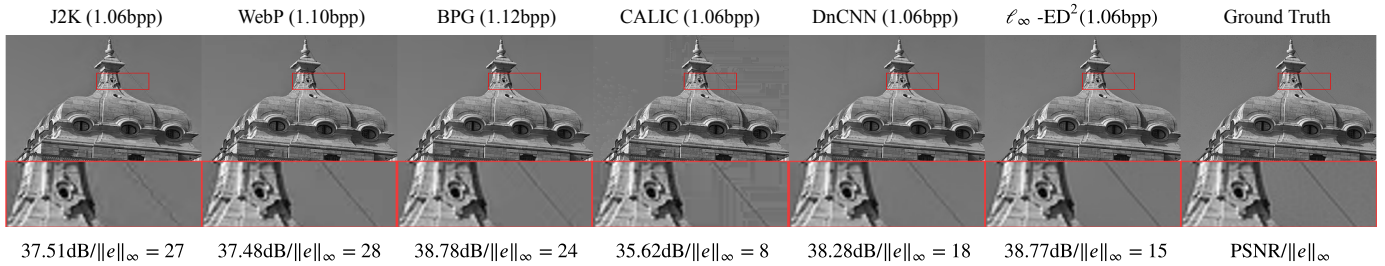


Fig. 10. Visual comparisons of different methods. Note the artifacts on and near the cable produced by J2K, WebP, BPG, CALIC and DnCNN in comparison with ℓ_∞ -ED² in close-up views, and also the correction of CALIC's patterned errors in smooth background by ℓ_∞ -ED².



Fig. 11. Visual comparisons of different methods. In the close-up views, note the ghost artifacts on the letters produced by J2K, WebP, BPG and DnCNN, and clean letter reconstruction by ℓ_∞ -ED².

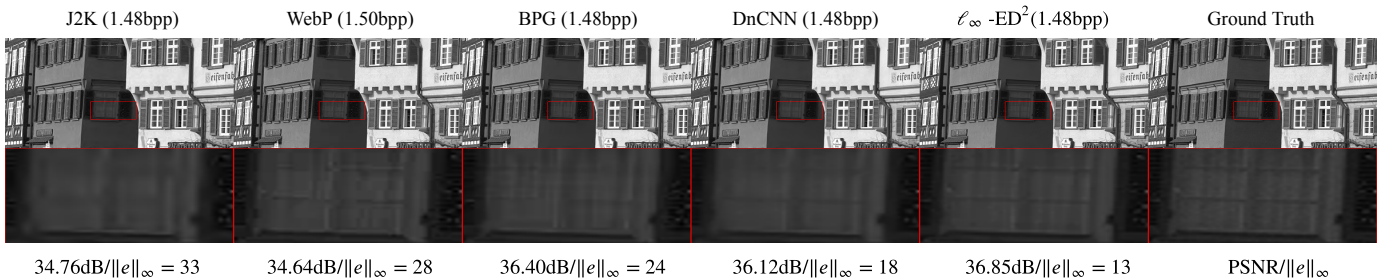


Fig. 12. Visual comparisons of different methods. In the close-up views, note the vertical window ripplefold drapery pattern and the horizontal window bars which are distorted by the J2K, WebP, BPG and DnCNN, but faithfully reconstructed by ℓ_∞ -ED².

B. Perceptual quality comparison

The perceptual qualities of competing methods, given the same bit rate, are compared in Figs. 8 through 12. Recall that our motivation is to devise a perceptually lossless image compression system that has a provable ℓ_∞ error bound. Therefore, the comparisons are made near the critical bit rate for perceptually transparent reconstruction. For each image the PSNR, ℓ_∞ error and the bit rate are stated.

The space shuttle test image (Fig. 8) is a telling example for the necessity of using the ℓ_∞ loss in ultra-high fidelity image compression in scientific and medical applications. The nuts on the shuttle hatch (see the green arrow in the ground truth image) are removed by WebP, BPG and DnCNN, which is an unacceptable semantic error. At the same bit rate the near-lossless CALIC preserves these nuts but it generates some false dots (marked by red arrow). Only the ℓ_∞ -ED² compression system is flawless.

In the second example of aerial image (Fig. 9), in the red window, the faint rectangular structure in the original image is completely erased by J2K, and it becomes illegible in the outputs of WebP, BPG and DnCNN due to severe blurring, while the ℓ_∞ -ED² system is able to recover the structure perfectly. In the blue window of Fig. 9, J2K almost erases the original parallel lines; the other competing methods are not satisfactory either with severe blurring and jaggy artifacts. Again, only the ℓ_∞ -ED² compression system achieves perceptually lossless reconstruction.

In the example of the roof top image (Fig. 10), all competing methods produce blurring, ghost and jaggy artifacts on the cable and roof contour in various degree, whereas the ℓ_∞ -ED² recovers the clean and sharp line and curves. Note how the structured compression artifacts of CALIC in smooth background are removed by the CNN-based soft decoding methods.

In Fig. 11, the letters restored by the ℓ_∞ -ED² compression system are much cleaner and sharper than other methods with a visually lossless quality with respect to the ground truth.

In Fig. 12, after zooming in, one can see that the ℓ_∞ -ED² compression system faithfully reconstructs the vertical window ripplefold drapery pattern and the horizontal window bars in the original image, but all other methods fail to do so, distorting the original patterns and structures noticeably.

Thanks to the ℓ_∞ minmax criterion, the proposed ℓ_∞ -SDNet soft decoding method can restore sharp edges and subtle features more accurately than the other methods, which explains its superior perceptual quality.

C. Ablation study

Quasi- ℓ_∞ loss and truncated activation In order to isolate the effects of imposing the ℓ_∞ loss, we build a baseline network of the same architecture as ℓ_∞ -SDNet but without the truncated activation module, and then train the baseline using only the MSE loss. The performance results of the baseline network on Kodak dataset are tabulated in Table VI in comparison with those of the proposed ℓ_∞ -SDNet. It can be seen that, after adding the quasi- ℓ_∞ loss and truncated activation, the network makes an appreciable performance

TABLE VI
PERFORMANCE RESULTS (PSNR/ $\|\epsilon\|_\infty$) OF THE ABLATION STUDIES ON THE KODAK DATASET.

BPP	Baseline	No dilation	Single-rate	ℓ_∞ -ED ²
2.61	50.20 / 2.00	50.21 / 2.00	50.24 / 2.00	50.26 / 2.00
1.98	46.32 / 4.00	46.29 / 4.00	46.37 / 4.00	46.42 / 4.00
1.60	44.06 / 6.00	44.05 / 5.95	44.12 / 5.84	44.19 / 5.83
1.35	42.48 / 8.00	42.41 / 7.76	42.51 / 7.30	42.61 / 7.29
1.19	41.24 / 9.89	41.15 / 9.54	41.29 / 9.11	41.38 / 9.04
1.03	40.09 / 11.74	40.01 / 11.12	40.19 / 10.88	40.29 / 10.79
0.91	39.12 / 13.65	39.06 / 12.96	39.25 / 12.48	39.36 / 12.38
0.82	38.24 / 15.68	38.21 / 14.78	38.42 / 14.25	38.55 / 14.16

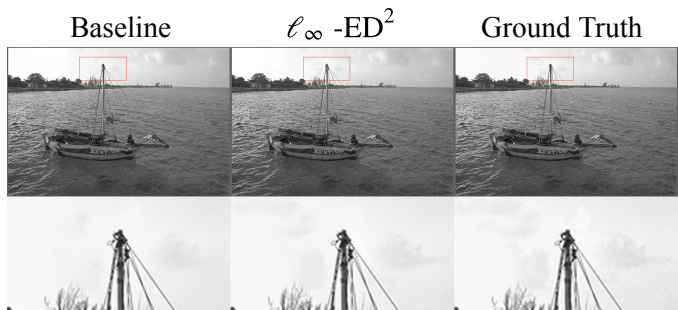


Fig. 13. Visual comparisons of different methods. Notice how the subtle clouds in the sky are almost erased by the baseline network, but well reconstructed by ℓ_∞ -SDNet.

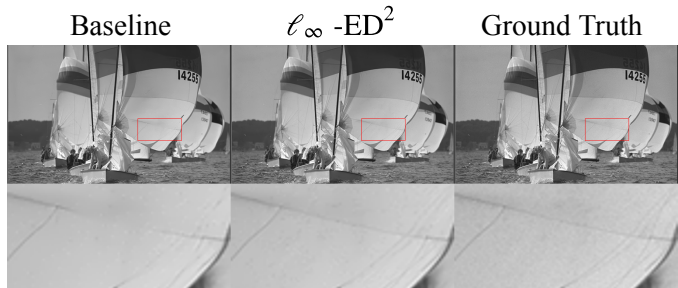


Fig. 14. Visual comparisons of different methods. Note the line on the sail which is broken by the baseline network, but recovered by the proposed ℓ_∞ -SDNet completely.

gain in PSNR and ℓ_∞ metric. We also provide the visual comparison results in Fig. 13 and 14. As shown in Fig. 13, the subtle clouds in the sky are almost erased by the baseline network, but are well reconstructed by ℓ_∞ -SDNet. In Fig. 14, the line on the sail is broken in the image recovered by the baseline, but it is recovered by ℓ_∞ -SDNet completely, even though the signal is very weak.

Dilated convolution We also conduct experiments to evaluate the effectiveness of the dilated convolution used in our network. We build a network by replacing the dilated convolution operation in ℓ_∞ -SDNet with the traditional convolution and train it with the same settings as in ℓ_∞ -SDNet. The performance results of using dilated convolution versus conventional convolution on Kodak dataset are compared in Table VI. As can be seen, the dilated convolution yields a small performance gain.

Multi-rate training To evaluate the universality of the proposed multi-rate training, we train eight rate-specific ℓ_∞ -SDNets for eight different rates and compare these single-rate CNNs with the proposed multi-rate ℓ_∞ -SDNet. Comparison results are shown in Table VI. It turns out, that the proposed multi-rate ℓ_∞ -SDNet is more robust than the single-rate counterpart. The multi-rate ℓ_∞ -SDNet even outperforms the single-rate ℓ_∞ -SDNet on testing images that are compressed at the said single rate.

VII. CONCLUSION

In this paper, we propose a novel image compression system of ℓ_∞ -constrained encoding coupled with CNN-based soft decoding (ℓ_∞ -ED²). The proposed ℓ_∞ -ED² approach beats the best of existing lossy image compression methods (e.g., BPG, WebP, etc.) not only in ℓ_∞ but also in ℓ_2 error metric and perceptual quality, for bit rates near the threshold of perceptually transparent reconstruction.

REFERENCES

- [1] X. Wu and N. Memon, "Calic-a context based adaptive lossless image codec," in *Acoustics, Speech, and Signal Processing, 1996. ICASSP-96. Conference Proceedings., 1996 IEEE International Conference on*, vol. 4. IEEE, 1996, pp. 1890–1893.
- [2] A. R. Calderbank, I. Daubechies, W. Sweldens, and B.-L. Yeo, "Lossless image compression using integer to integer wavelet transforms," in *Image Processing, 1997. Proceedings., International Conference on*, vol. 1. IEEE, 1997, pp. 596–599.
- [3] X. Wu and N. Memon, "Context-based, adaptive, lossless image coding," *IEEE transactions on Communications*, vol. 45, no. 4, pp. 437–444, 1997.
- [4] S. Maniccam and N. G. Bourbakis, "Lossless image compression and encryption using scan," *Pattern Recognition*, vol. 34, no. 6, pp. 1229–1245, 2001.
- [5] N. V. Boulgouris, D. Tzovaras, and M. G. Strintzis, "Lossless image compression based on optimal prediction, adaptive lifting, and conditional arithmetic coding," *IEEE Transactions on Image Processing*, vol. 10, no. 1, pp. 1–14, 2001.
- [6] L. Ke and M. W. Marcellin, "Near-lossless image compression: minimum-entropy, constrained-error dpcm," *IEEE Transactions on Image Processing*, vol. 7, no. 2, pp. 225–228, 1998.
- [7] I. Avcibas, N. Memon, B. Sankur, and K. Sayood, "A progressive lossless/near-lossless image compression algorithm," *IEEE Signal Processing Letters*, vol. 9, no. 10, pp. 312–314, 2002.
- [8] K. Chen and T. V. Ramabadran, "Near-lossless compression of medical images through entropy-coded dpcm," *IEEE Transactions on Medical Imaging*, vol. 13, no. 3, pp. 538–548, 1994.
- [9] X. Wu, W. K. Choi, and P. Bao, " L_∞ constrained high-fidelity image compression via adaptive context modeling," in *Data Compression Conference, 1997. DCC'97. Proceedings.* IEEE, 1997, pp. 91–100.
- [10] W. B. Pennebaker and J. L. Mitchell, *JPEG: Still image data compression standard.* Springer Science & Business Media, 1992.
- [11] J. Zhou, X. Wu, and L. Zhang, " ℓ_2 restoration of ℓ_∞ -decoded images via soft-decision estimation," *IEEE transactions on image processing*, vol. 21, no. 12, pp. 4797–4807, 2012.
- [12] C. Dong, Y. Deng, C. Change Loy, and X. Tang, "Compression artifacts reduction by a deep convolutional network," in *Proceedings of the IEEE International Conference on Computer Vision*, 2015, pp. 576–584.
- [13] L. Galteri, L. Seidenari, M. Bertini, and A. Del Bimbo, "Deep generative adversarial compression artifact removal," *arXiv preprint arXiv:1704.02518*, 2017.
- [14] J. Guo and H. Chao, "One-to-many network for visually pleasing compression artifacts reduction," *arXiv preprint arXiv:1611.04994*, 2016.
- [15] D. Minnen, J. Ballé, and G. D. Toderici, "Joint autoregressive and hierarchical priors for learned image compression," in *Advances in Neural Information Processing Systems*, 2018, pp. 10771–10780.
- [16] E. Agustsson, M. Tschannen, F. Mentzer, R. Timofte, and L. Van Gool, "Generative adversarial networks for extreme learned image compression," *arXiv preprint arXiv:1804.02958*, 2018.
- [17] M. Li, W. Zuo, S. Gu, D. Zhao, and D. Zhang, "Learning convolutional networks for content-weighted image compression," in *Proceedings of the IEEE Conference on Computer Vision and Pattern Recognition*, 2018, pp. 3214–3223.
- [18] F. Mentzer, E. Agustsson, M. Tschannen, R. Timofte, and L. Van Gool, "Conditional probability models for deep image compression," in *Proceedings of the IEEE Conference on Computer Vision and Pattern Recognition*, 2018, pp. 4394–4402.
- [19] A. Foi, V. Katkovnik, and K. Egiazarian, "Pointwise shape-adaptive dct for high-quality denoising and deblocking of grayscale and color images," *IEEE Transactions on Image Processing*, vol. 16, no. 5, pp. 1395–1411, 2007.
- [20] X. Zhang, R. Xiong, X. Fan, S. Ma, and W. Gao, "Compression artifact reduction by overlapped-block transform coefficient estimation with block similarity," *IEEE transactions on image processing*, vol. 22, no. 12, pp. 4613–4626, 2013.
- [21] Y. Li, F. Guo, R. T. Tan, and M. S. Brown, "A contrast enhancement framework with jpeg artifacts suppression," in *European Conference on Computer Vision*. Springer, 2014, pp. 174–188.
- [22] H. Chang, M. K. Ng, and T. Zeng, "Reducing artifacts in jpeg de-compression via a learned dictionary," *IEEE transactions on signal processing*, vol. 62, no. 3, pp. 718–728, 2014.
- [23] Y. Dar, A. M. Bruckstein, M. Elad, and R. Giryes, "Postprocessing of compressed images via sequential denoising," *IEEE Transactions on Image Processing*, vol. 25, no. 7, pp. 3044–3058, 2016.
- [24] H. C. Reeve and J. S. Lim, "Reduction of blocking effects in image coding," *Optical Engineering*, vol. 23, no. 1, p. 230134, 1984.
- [25] G. Zhai, W. Zhang, X. Yang, W. Lin, and Y. Xu, "Efficient image deblocking based on postfiltering in shifted windows," *IEEE Transactions on Circuits and Systems for Video Technology*, vol. 18, no. 1, pp. 122–126, 2008.
- [26] F. Alter, S. Durand, and J. Froment, "Adapted total variation for artifact free decompression of jpeg images," *Journal of Mathematical Imaging and Vision*, vol. 23, no. 2, pp. 199–211, 2005.
- [27] K. Bredies and M. Holler, "A total variation-based jpeg decompression model," *SIAM Journal on Imaging Sciences*, vol. 5, no. 1, pp. 366–393, 2012.
- [28] X. Liu, X. Wu, J. Zhou, and D. Zhao, "Data-driven soft decoding of compressed images in dual transform-pixel domain," *IEEE Transactions on Image Processing*, vol. 25, no. 4, pp. 1649–1659, 2016.
- [29] P. Svoboda, M. Hradis, D. Barina, and P. Zemcik, "Compression artifacts removal using convolutional neural networks," *arXiv preprint arXiv:1605.00366*, 2016.
- [30] W. Zuo, K. Zhang, and L. Zhang, *Convolutional Neural Networks for Image Denoising and Restoration*. Cham: Springer International Publishing, 2018, pp. 93–123. [Online]. Available: https://doi.org/10.1007/978-3-319-96029-6_4
- [31] Y. Zhang, Y. Tian, Y. Kong, B. Zhong, and Y. Fu, "Residual dense network for image restoration," *arXiv preprint arXiv:1812.10477*, 2018.
- [32] X.-J. Mao, C. Shen, and Y.-B. Yang, "Image restoration using convolutional auto-encoders with symmetric skip connections," *arXiv preprint arXiv:1606.08921*, 2016.
- [33] B. Lim, S. Son, H. Kim, S. Nah, and K. Mu Lee, "Enhanced deep residual networks for single image super-resolution," in *Proceedings of the IEEE conference on computer vision and pattern recognition workshops*, 2017, pp. 136–144.
- [34] M. Haris, G. Shakhnarovich, and N. Ukita, "Deep back-projection networks for super-resolution," in *Proceedings of the IEEE conference on computer vision and pattern recognition*, 2018, pp. 1664–1673.
- [35] Y. Zhang, K. Li, K. Li, L. Wang, B. Zhong, and Y. Fu, "Image super-resolution using very deep residual channel attention networks," in *Proceedings of the European Conference on Computer Vision (ECCV)*, 2018, pp. 286–301.
- [36] K. He, X. Zhang, S. Ren, and J. Sun, "Deep residual learning for image recognition," in *Proceedings of the IEEE conference on computer vision and pattern recognition*, 2016, pp. 770–778.
- [37] F. Yu and V. Koltun, "Multi-scale context aggregation by dilated convolutions," *arXiv preprint arXiv:1511.07122*, 2015.
- [38] T. Wang, M. Sun, and K. Hu, "Dilated deep residual network for image denoising," in *2017 IEEE 29th International Conference on Tools with Artificial Intelligence (ICTAI)*. IEEE, 2017, pp. 1272–1279.
- [39] W. Shi, F. Jiang, and D. Zhao, "Single image super-resolution with dilated convolution based multi-scale information learning inception module," in *2017 IEEE International Conference on Image Processing (ICIP)*. IEEE, 2017, pp. 977–981.
- [40] D. P. Kingma and J. Ba, "Adam: A method for stochastic optimization," *arXiv preprint arXiv:1412.6980*, 2014.

- [41] M. Abadi, A. Agarwal, P. Barham, E. Brevdo, Z. Chen, C. Citro, G. S. Corrado, A. Davis, J. Dean, M. Devin, S. Ghemawat, I. Goodfellow, A. Harp, G. Irving, M. Isard, Y. Jia, R. Jozefowicz, L. Kaiser, M. Kudlur, J. Levenberg, D. Mané, R. Monga, S. Moore, D. Murray, C. Olah, M. Schuster, J. Shlens, B. Steiner, I. Sutskever, K. Talwar, P. Tucker, V. Vanhoucke, V. Vasudevan, F. Viégas, O. Vinyals, P. Warden, M. Wattenberg, M. Wicke, Y. Yu, and X. Zheng, "TensorFlow: Large-scale machine learning on heterogeneous systems," 2015, software available from tensorflow.org. [Online]. Available: <http://tensorflow.org/>
- [42] A. Skodras, C. Christopoulos, and T. Ebrahimi, "The jpeg 2000 still image compression standard," *IEEE Signal processing magazine*, vol. 18, no. 5, pp. 36–58, 2001.
- [43] Google, "A new image format for the web," <https://developers.google.com/speed/webp/>.
- [44] F. Bellard, "Better portable graphics (bpg)," <https://bellard.org/bpg/>.
- [45] H. R. Sheikh, M. F. Sabir, and A. C. Bovik, "A statistical evaluation of recent full reference image quality assessment algorithms," *IEEE Transactions on image processing*, vol. 15, no. 11, pp. 3440–3451, 2006.
- [46] Kodak, "Kodak lossless true color image suite," <http://r0k.us/graphics/kodak/>.
- [47] J.-B. Huang, A. Singh, and N. Ahuja, "Single image super-resolution from transformed self-exemplars," in *Proceedings of the IEEE Conference on Computer Vision and Pattern Recognition*, 2015, pp. 5197–5206.